

1 **Microstructures in shocked quartz: linking nuclear airbursts and** 2 **meteorite impacts**

3
4 Robert E. Hermes, Hans-Rudolf Wenk, James P. Kennett, Ted E. Bunch, Christopher R. Moore,
5 Malcolm A. LeCompte, Gunther Kletetschka, A. Victor Adedeji, Kurt Langworthy, Joshua Razink,
6 Valerie Brogden, Brian van Devener, Jesus Paulo Perez, Randy Polson, Matt Nowell, Allen West
7

8 **TEXT, METHODS**

9 **SAMPLES**

10 **METEOR CRATER.** This sample was collected in 1966 by co-author T.E.B. on the rim
11 ~500 m north of the crater's center at ~35.032206° N, 111.023988° W.

12 **JOE-1/4.** This sample was obtained in 2011 at the Semipalatinsk test site by Dr. Byron
13 Ristvet, DTRA, with permission from the Kazakhstan National Nuclear Center and the Russian
14 Federation Atomic Energy Agency. The bulk sample was sifted to obtain the fine sand studied.

15 **TRINITY.** A sediment sample “JIE” was obtained in 2003 at the Trinity Site near ground
16 zero by Jim Eckles of the White Sands Missile Range Public Affairs Office. The gross sample was
17 sifted to remove fines as well as larger rocks. The resulting sand fraction was used to produce the
18 thin-sectioned slides for this investigation. The “meltglass” sample was obtained in 2011 at the
19 Trinity Site about 400 meters NNE from ground zero, where it landed following ejection by the
20 detonation. Co-author R.E.H. collected it with permission from the White Sands Missile Range
21 Public Affairs office, and part of it was thin-sectioned for this study.
22

23 **PROCESSING STEPS**

- 24 (i) Sediment was wet-sieved to concentrate grains between diameters of ~150 (#100 ASTM
25 sieve) to ~850 μm (#20 ASTM sieve).
- 26 (ii) Typically, the sorted grains were treated with HCl to remove carbonates.
- 27 (iii) Grains were embedded in blue epoxy for better visibility, covering the entire 27 x 46 mm
28 slide, and were sectioned at Spectrum Petrographics, Vancouver, WA. Sectioned slides were
29 given a high-polish, microprobe-grade finish necessary for EBSD analyses. No cover slide
30 was used.
- 31 (iv) Slides were etched with HF vapor at 50% concentration for ~2 min. Note that exposure for
32 <2 min was insufficient for etching and exposing shock fractures; exposure for >2 min can
33 damage the slides.
- 34 (v) Grains were examined using a petrographic polarizing microscope with a rotary stage. The
35 microscope was equipped with transmitted light and epi-illumination (reflected light). First,
36 epi-illumination was used, and then transmitted light was used with objectives ranging from
37 04x to 100x magnification. Once a candidate grain was identified, it was rotated to extinction
38 under cross polars. Photomicrographs were acquired under both transmitted light and epi-
39 illumination.

- 40 (vi) SEM imaging was performed after re-polishing the etched grains to a microprobe finish
41 using 50 nm colloidal silica.
- 42 (vii) Next, the elemental compositions of individual grains were determined using SEM-based
43 EDS.
- 44 (viii) Cathodoluminescence was recorded in both panchromatic (185–850 nm wavelengths) and
45 3-filtered (RGB) formats. Because red, green, and blue channels were optimized individually
46 to obtain the maximum amount of information from the image, color information in the
47 images is non-quantitative.
- 48 (ix) EBSD analyses were performed using multiple routines.
- 49 (x) FIB foils were extracted from selected quartz grains.
- 50 (xi) TEM analyses were performed on individual foils.
- 51 (xii) Elemental compositions of the grains were determined using TEM-based EDS. FFTs and bi-
52 plots of d-spacing and intensity were produced with Digital Micrograph, version
53 3.32.2403.0. Because electron microscopy is capable of causing irradiation-induced
54 amorphization[1], quartz grains were examined at low magnification using low voltages and
55 short image-acquisition times.
- 56

57 ANALYTICAL DETAILS

58 **HF ETCHING.** Following Bunch et al.[2], Spectrum Petrographics, Vancouver, WA,
59 etched thin-sectioned slides by exposure to HF vapor for 2 min to dissolve amorphous quartz and
60 make any lamellae more visible. After treatment with HF vapor, we performed another dH₂O rinse.

61 Alternately, we treated some slides with liquid HF for 2 min, after which we performed a
62 dH₂O rinse; neutralized them with 5% sodium carbonate solution; rinsed them with dH₂O again;
63 then treated them with 5% HCl to remove carbonates. The HF vapor produced more consistent
64 results than liquid HF. Multiple studies[3-8] have demonstrated the utility of etching quartz grains
65 with HF to differentiate between glass-filled shock features and glass-free tectonic deformation
66 lamellae. In our study, we observed that HF sometimes lightly etches tectonic deformation
67 lamellae to reveal broad, shallow depressions, as others reported[5,7]. However, unlike shock
68 fractures, these depressions in the damaged lattice did not extend more than a few microns into the
69 grain and were not observed to contain amorphous silica.

70 **SEM AND SEM-EDS.** At Elizabeth City State University, North Carolina, analyses were
71 conducted in low-vacuum mode using a JEOL-6000 SEM system. At the University of Oregon,
72 we used a ThermoFisher Apreo 2 SEM with a CL detector. Using SEM-EDS, we manually selected
73 for detection of major elements with uncertainties of approximately $\pm 10\%$. At the University of
74 Utah, secondary and backscattered electron images were collected using a Teneo SEM system
75 (Thermofisher FEI, Hillsboro, OR).

76 **TEM, STEM, and TEM-EDS.** At the CAMCOR facility at the University of Oregon,
77 Transmission/Scanning transmission electron microscopy, or (S)TEM, was performed on an FEI
78 80-300 Titan scanning/transmission electron microscope (STEM) equipped with an image
79 corrector, High-Angle Annular Dark Field (HAADF) detector, Energy Dispersive X-ray

80 Spectroscopy (EDS) detector, Gatan Imaging Filter (GIF), and a 4-megapixel Charge-Coupled
81 Device (CCD) camera. Microscope magnification was calibrated using a standard cross-grating
82 carbon replica (2,160 lines/mm) evaporated with Au-Pd (Ted Pella #607). All images, diffraction
83 patterns, and EDX maps were collected at 300Kv and processed using Digital Micrograph, version
84 3.32.2403.0.

85 STEM/TEM was performed on a JEOL 2800 operated at 200 kV at the University of Utah.
86 EDS data was collected and processed using ThermoFisher Noran System 7 software. Spectral
87 maps were processed as net-counts (background subtracted) using a 5x5 kernel size. Quantitative
88 results were obtained using the Cliff-Lorimer method with absorption correction.

89 **FOCUSED ION BEAM.** At the CAMCOR facility of the University of Oregon, TEM
90 samples of quartz foils were prepared using a Helios Dual Beam SEM FIB. At the Surface Analysis
91 Laboratory at the University of Utah, TEM sample preparation of quartz foils from bulk specimens
92 was performed on an FEI/Thermo Helios Nanolab 650. The lift-out procedure followed standard
93 sample preparation techniques. An electron beam deposited platinum layer as first locally
94 deposited. Next, an ion-beam platinum layer was deposited. Trenches were milled on each side of
95 the protective layer. Cuts were then made to the underside, and a micromanipulator probe was
96 placed in contact with the surface (Omniprobe 200). The probe was attached by depositing
97 platinum, and then the sample was cut free from the bulk. After using the micromanipulator probe,
98 the lift-out was attached to a copper support grid. The sample was then thinned using the ion beam
99 at progressively decreasing accelerating voltages, 30kV, 16kV, 8kV, and 2kV.

100 **CATHODOLUMINESCENCE.** At the University of Oregon, cathodoluminescent (CL)
101 images were synchronously captured at red (R), green (G), and blue (B) wavelengths on coated
102 thin sections in low-vacuum mode on a Thermo Apreo2 S FE-SEM at 10kV using 3.2nA of beam
103 current at ~10 mm working distance with 50Pa of chamber pressure to balance charge. Individual
104 images using red, blue, and green wavelength filters on the CL detector were acquired and
105 composited to create a 24-bit color image. Wavelength ranges: red: 595-813 nm; green: 495-615;
106 and blue: 291-509 nm. Backscatter (BSE) and secondary (SE) electron images were captured with
107 similar beam settings.

108 **EBS.** At the University of California, Berkeley, SEM analyses were performed with a
109 Zeiss EVO for imaging operated at 20 kV and EDS analyses used an EDAX-AMETEK
110 spectrometer with corresponding Genesis software. EBSD mapping used a Digiview detector and
111 TSL-OIM software. At the University of Utah, a Velocity Super EBSD camera (EDAX,
112 Pleasanton, CA) was used to collect diffracted electrons for crystal structure analysis.

113 At the University of Utah, secondary and backscattered electron SEM images were
114 collected using a Teneo system (Thermofisher FEI; Hillsboro, OR). EDS, EBSD, and CL analyses
115 were similarly conducted with the same SEM system installed with the following detectors. An
116 Octane Elite EDS system (EDAX, Pleasanton, CA) was used to collect elemental spectra. A
117 Monarc CL Detector (Gatan; Pleasanton, CA) was used for cathodoluminescence studies. SEM
118 beam energy and current were optimized to meet the requirements of each analysis mode. Before
119 imaging, sample slides were polished to 0.20 μm roughness with colloidal silica suspension and
120 washed with water to remove residues. The slides were then coated with 5-nm-thick carbon using

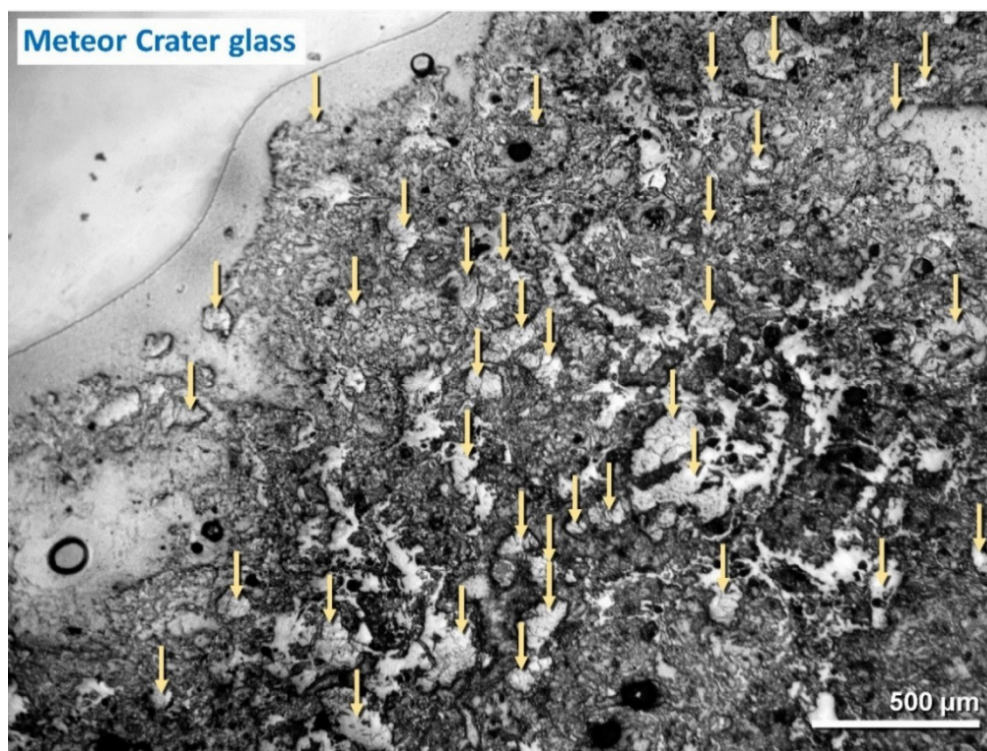
121 a Leica EM ACE600 coater (Leica Microsystems, Inc., Deerfield, IL) to prevent charging during
122 the imaging process.

123 **MICRO-RAMAN.** We investigated the shock fractures using micro-Raman with poor
124 results. Even after highly polishing the quartz grains, their extensive fractures and amorphization
125 made it challenging to acquire Raman spectra.

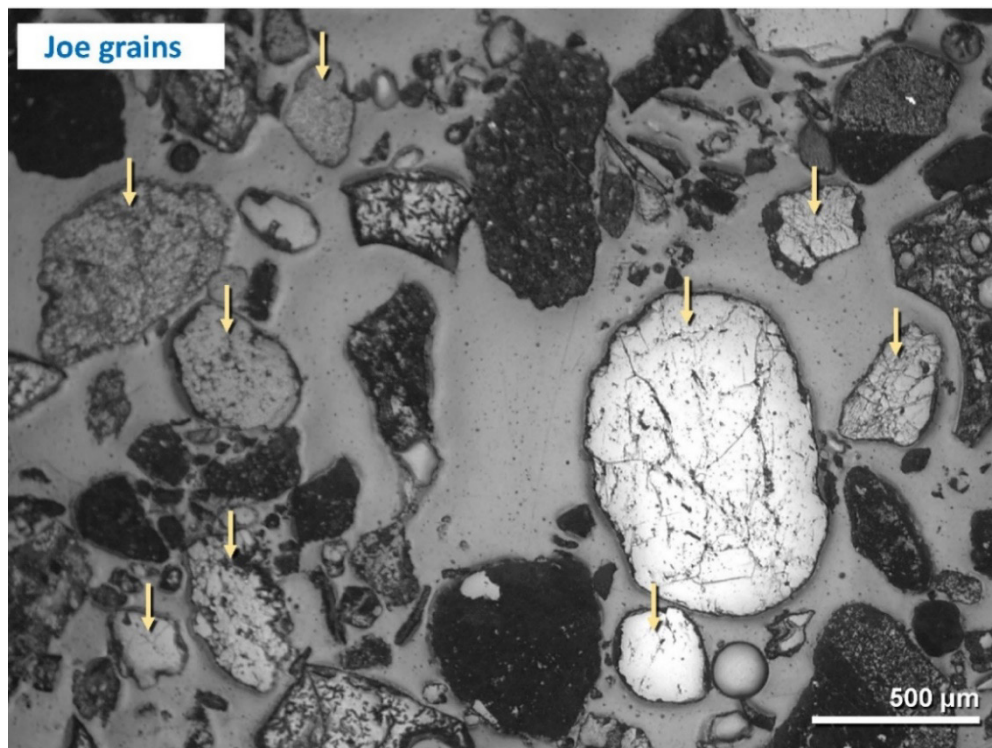
126 **UNIVERSAL STAGE.** We also investigated the shock fractures using the universal stage.
127 However, we could not determine Miller indices because the observed shock fractures are non-
128 planar and, thus, cannot be accurately measured and compared to planar features.

129
130 **FIGURES**

131



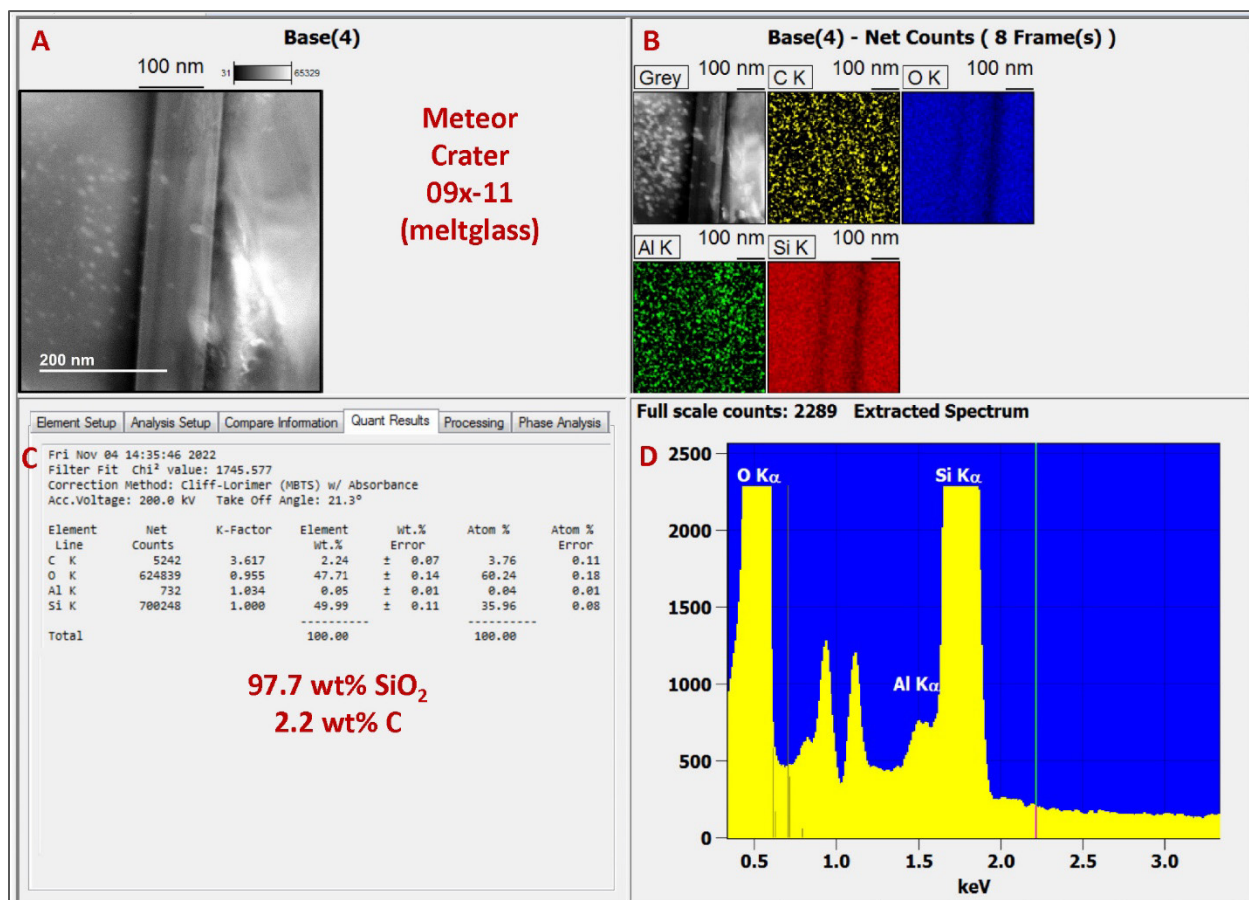
132
133 **Figure S1. Meltglass containing shock-fractured quartz from Meteor Crater.** Epi-
134 photomicrograph of a thin-sectioned slide. We analyzed ~36 quartz grains (arrows) displaying
135 shock fractures in a fragment of ejected meltglass. Shock-fractured grains were concentrated at
136 ~600 quartz grains per cm².
137



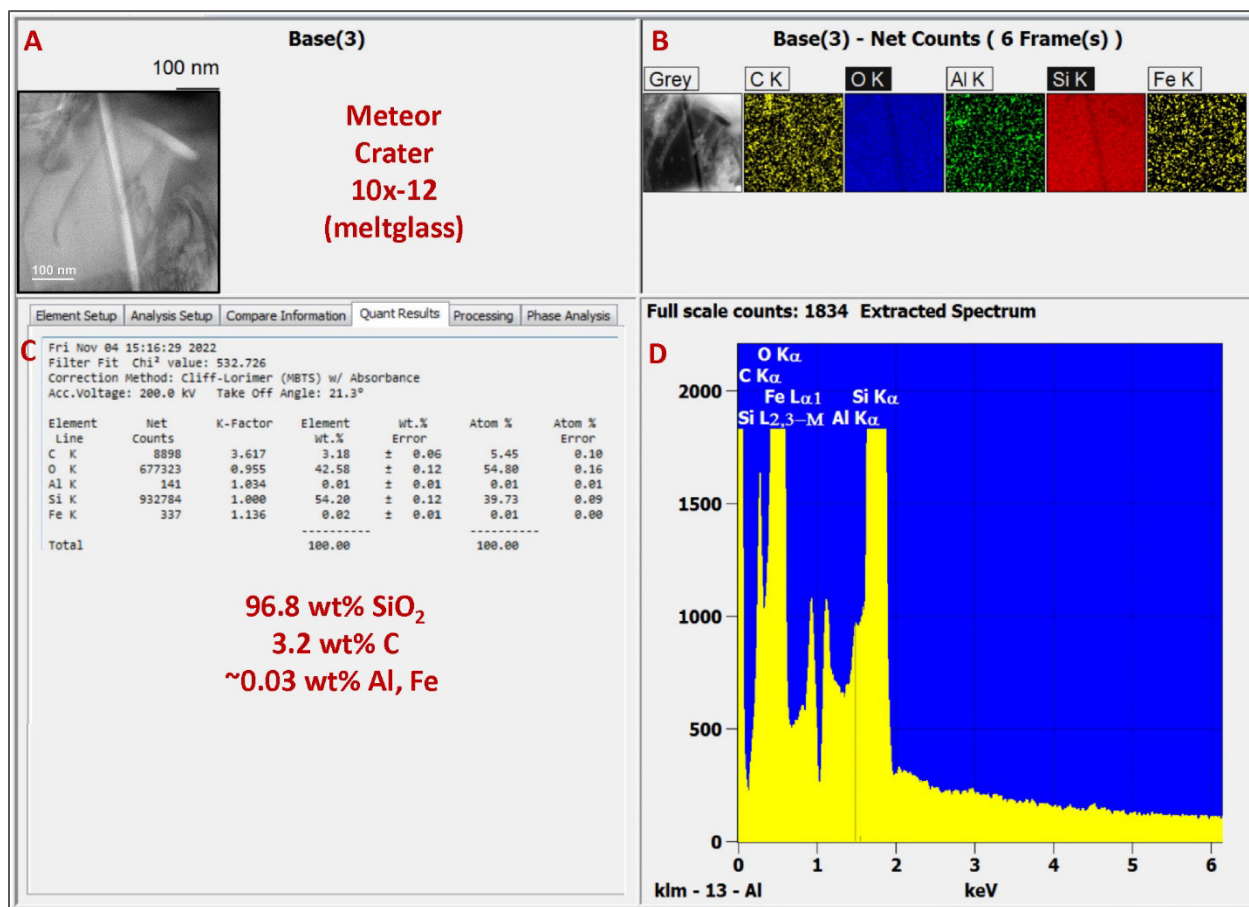
138
 139 **Figure S2. Shock-fractured quartz grains from the Joe-1/4 atomic test site.** Epi-
 140 photomicrograph of a thin-sectioned slide. We analyzed ~24 loose grains (9 shown at arrows) with
 141 shock fractures. Extracted from test site sediment at a concentration of ~150 quartz grains per cm².



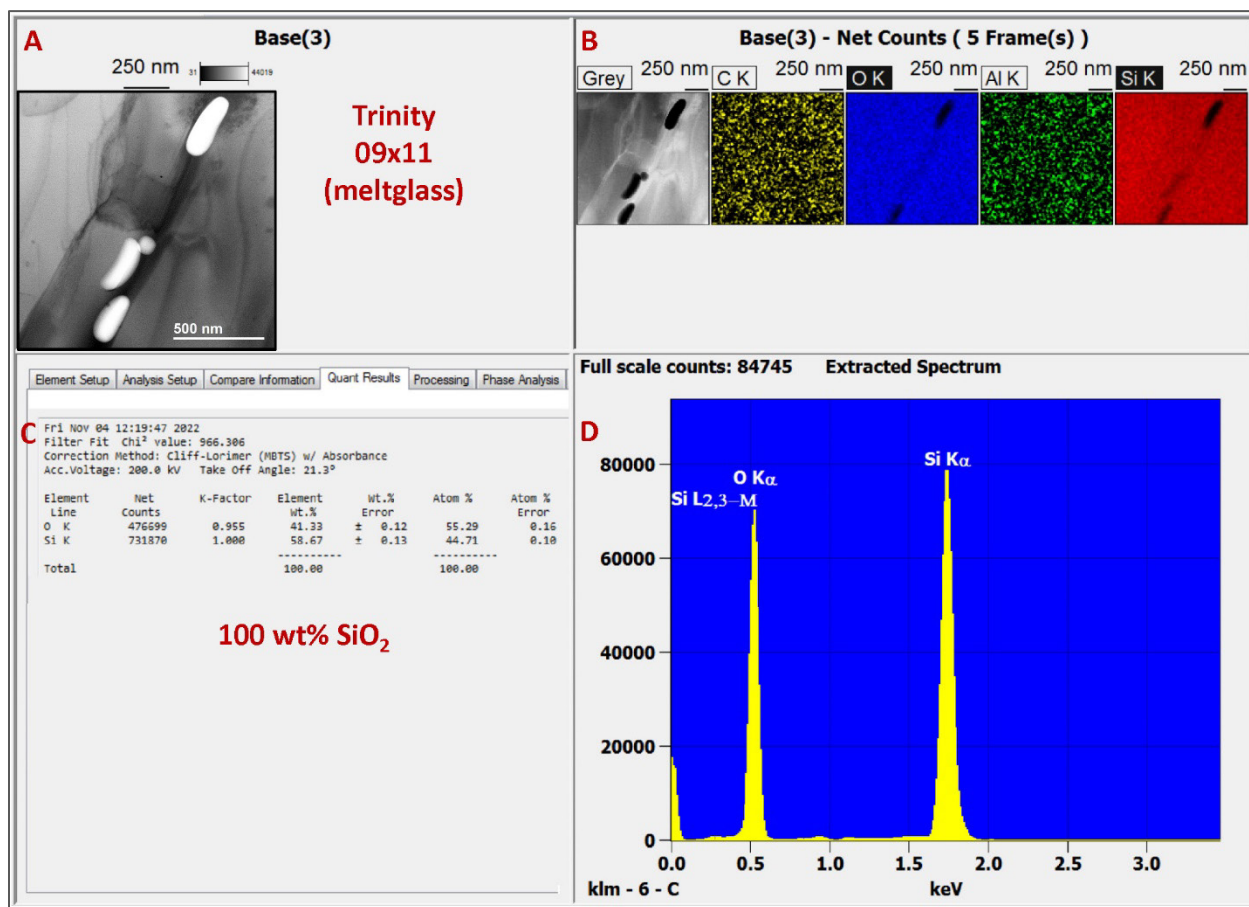
142
 143 **Figure S3. Shock-fractured quartz grains in Trinity meltglass.** Epi-photomicrograph of a thin-
 144 sectioned slide. We analyzed 42 grains (arrows) with shock fractures from ejected meltglass at a
 145 concentration of ~700 quartz grains per cm².



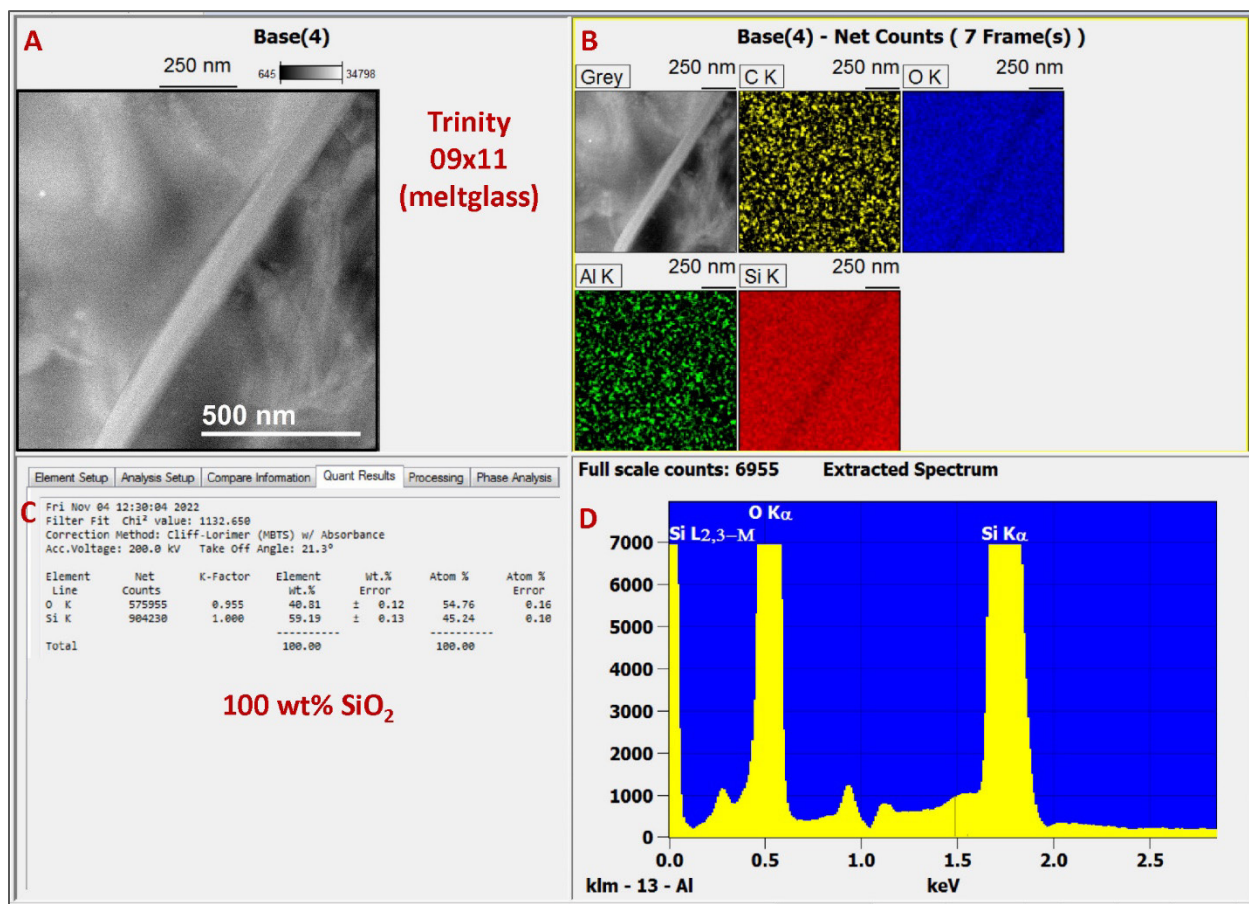
146
 147 **Figure S4. TEM-EDS data for Meteor Crater grain 09x-11. 97.7 wt% SiO₂, 2.2 wt% C, and**
 148 **0.05 wt% Al. Note that the C and Al are distributed evenly across the foil, suggesting**
 149 **contamination from processing the sample. (A) TEM image showing area with amorphous silica**
 150 **(center) in the grain. EDS analyses were made on the entire field of view. (B) Panels showing**
 151 **concentrations of selected elements. (C) Elemental concentrations were measured for the entire**
 152 **field of view. (D) Energy spectrum for various elements of EDS analysis. These descriptions also**
 153 **apply to captions for Figs. S7-S9 below.**



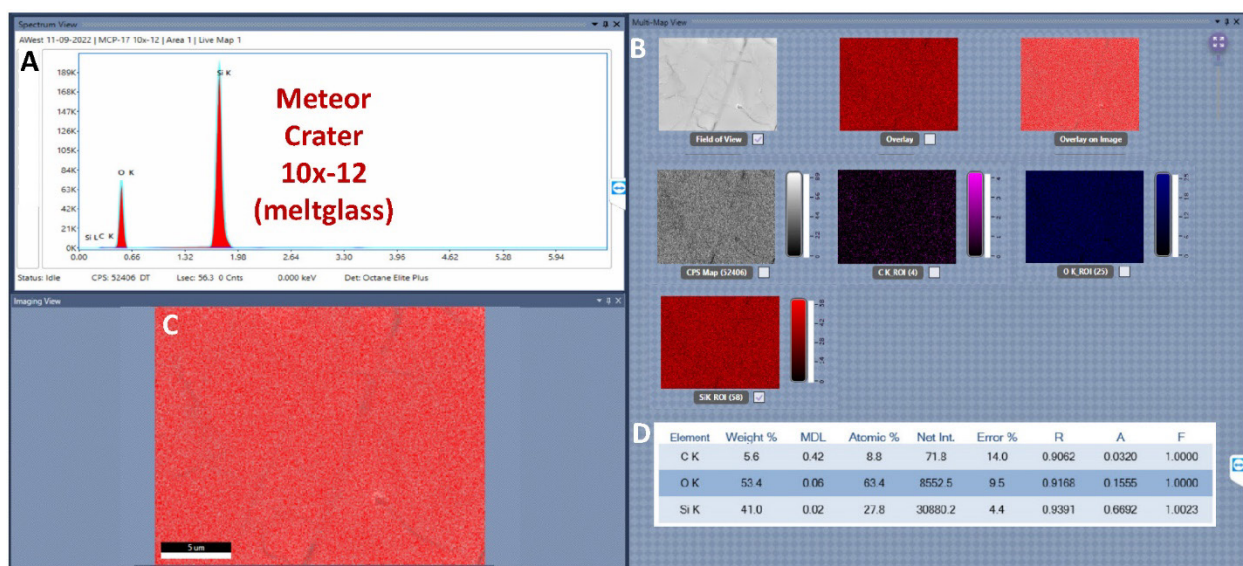
154
155 **Figure S5. TEM-EDS data for Meteor Crater grain 10x-12. 96.8 wt% SiO₂, 3.2 wt% C, 0.02**
156 **wt% Fe, and 0.01 wt% Al. Note that the C, Fe, and Al appear to be contaminants introduced during**
157 **the processing of the sample. For descriptions of panels, see the caption for Fig. S6.**



158
159 **Figure S6. TEM-EDS data for Trinity meltglass grain 09x11. ~100 wt% SiO₂ with negligible**
160 **amounts of Al and C, most likely contamination from processing the sample. For descriptions of**
161 **panels, see the caption for Fig. S6.**

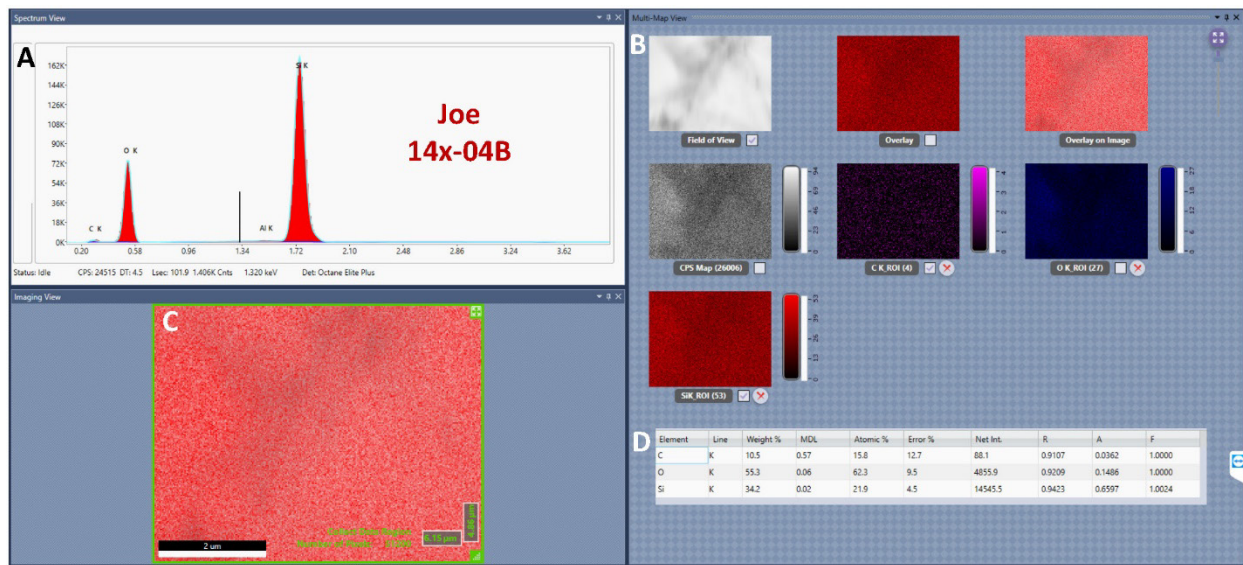


162
 163 **Figure S7. Additional TEM-EDS data for Trinity meltglass grain 09x11. ~100 wt% SiO₂ with**
 164 **insignificant amounts of Al and C, most likely contamination from processing the sample. For**
 165 **descriptions of panels, see the caption for Fig. S6.**
 166

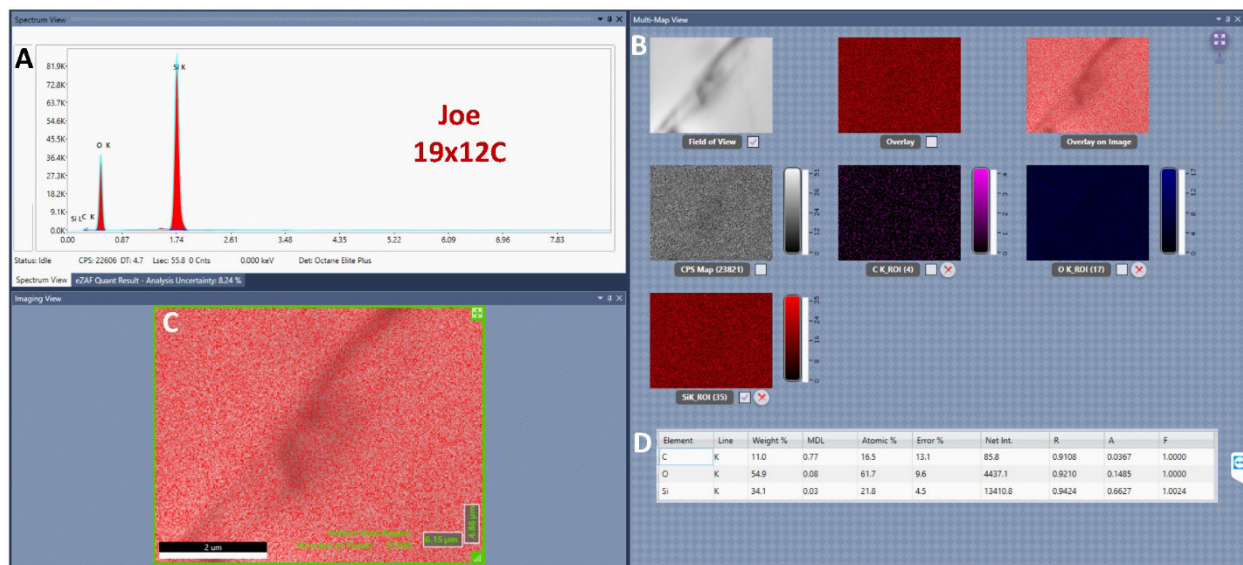


167
 168 **Figure S8. SEM-based EDS spectrum for Meteor crater grain 10x-12. (A) Energy spectrum**
 169 **for various elements of EDS analysis. EDS analyses were made on the entire field of view. (B)**
 170 **Panels showing concentrations of selected elements. (C) Composite image showing silicon panel**

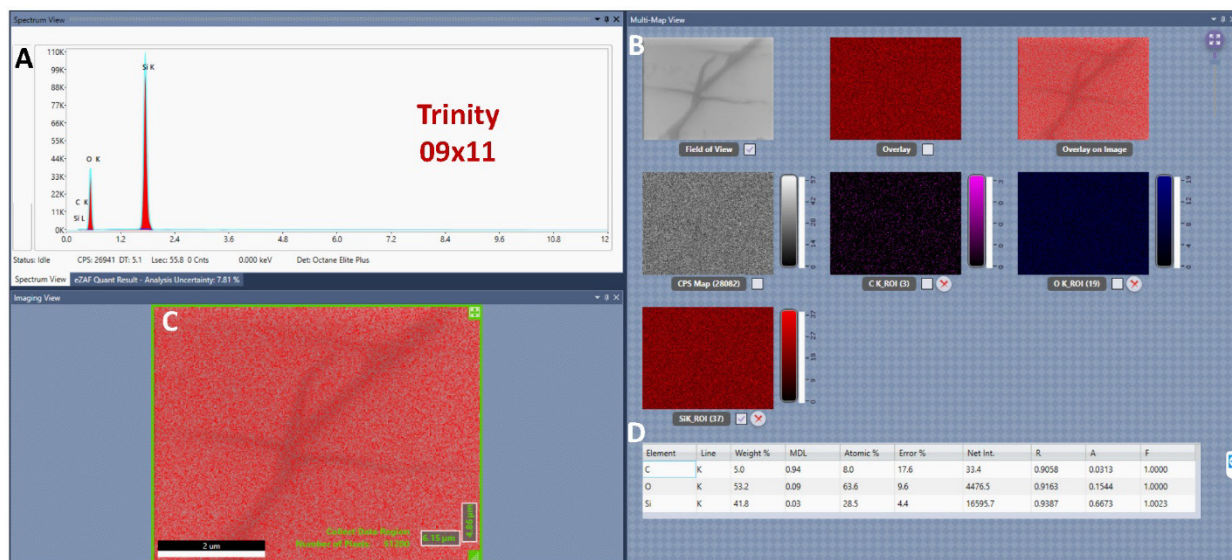
171 overlying the SEM field of view. **(D)** Elemental concentrations were measured for the entire field
 172 of view. These descriptions also apply to captions for **Figs. S11-S14** below.
 173



174
 175 **Figure S9. SEM-based EDS spectrum for Joe-1/4 grain 14x-04B.** For descriptions of panels
 176 **(A)-(D)**, see the caption for **Fig. S10**.
 177

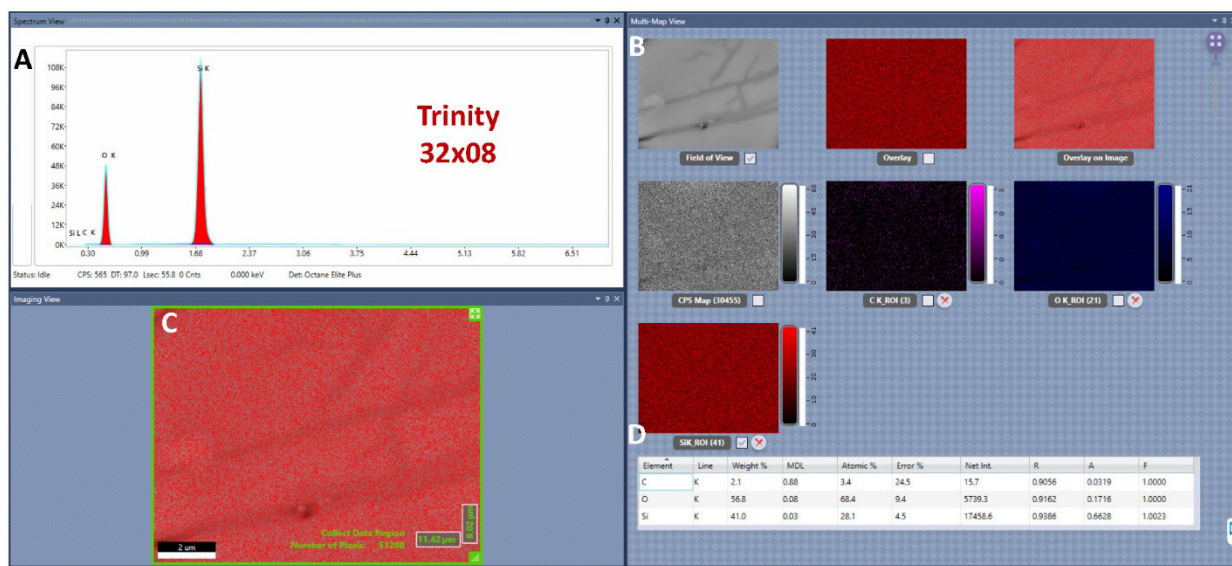


178
 179 **Figure S10. SEM-based EDS spectrum for Joe-1/4 grain 19x-12C.** For descriptions of panels
 180 **(A)-(D)**, see the caption for **Fig. S10**.
 181

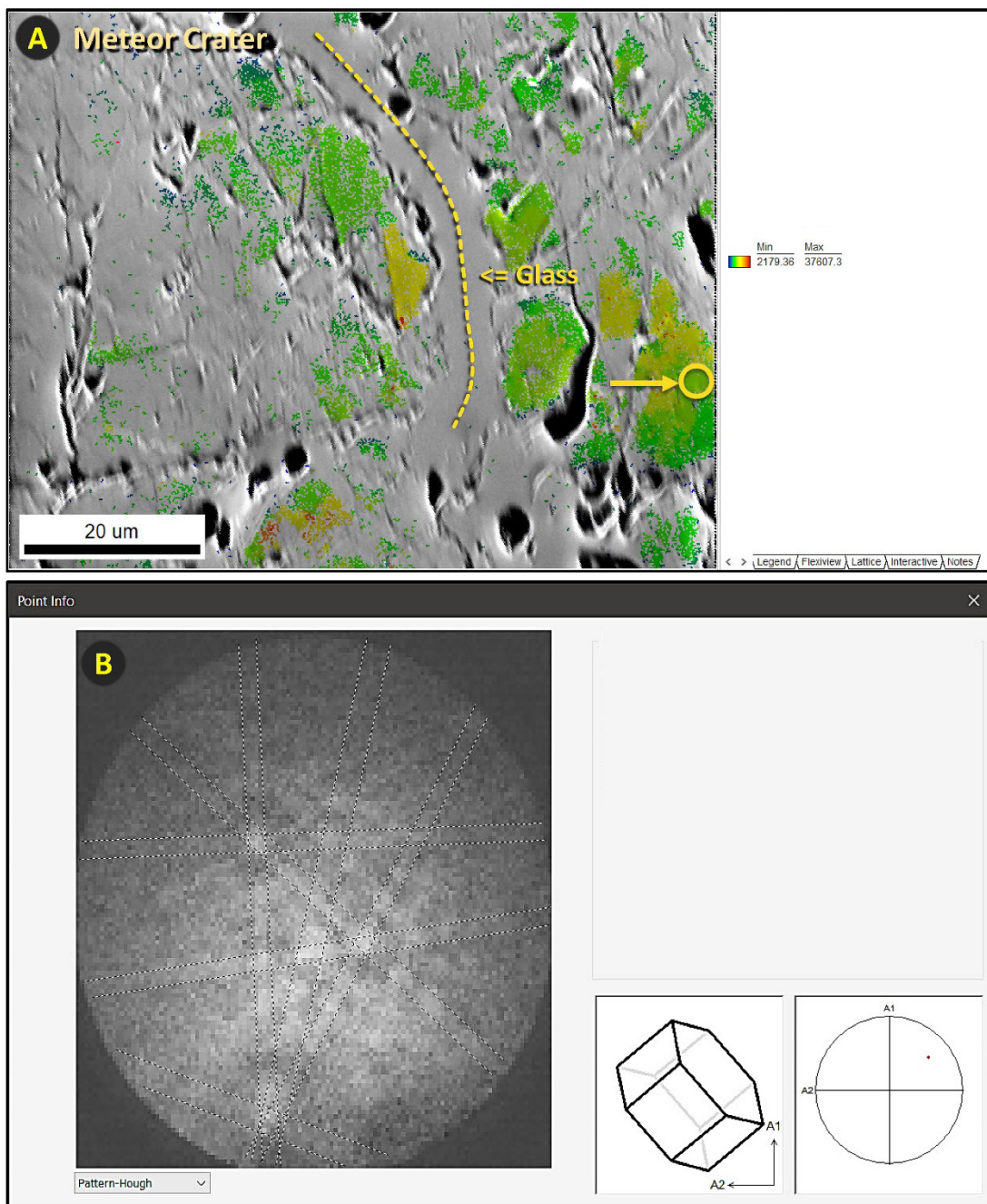


182
 183 **Figure S11. SEM-based EDS spectrum for Trinity meltglass grain 09x11.** For descriptions of
 184 panels (A)-(D), see the caption for Fig. S10.

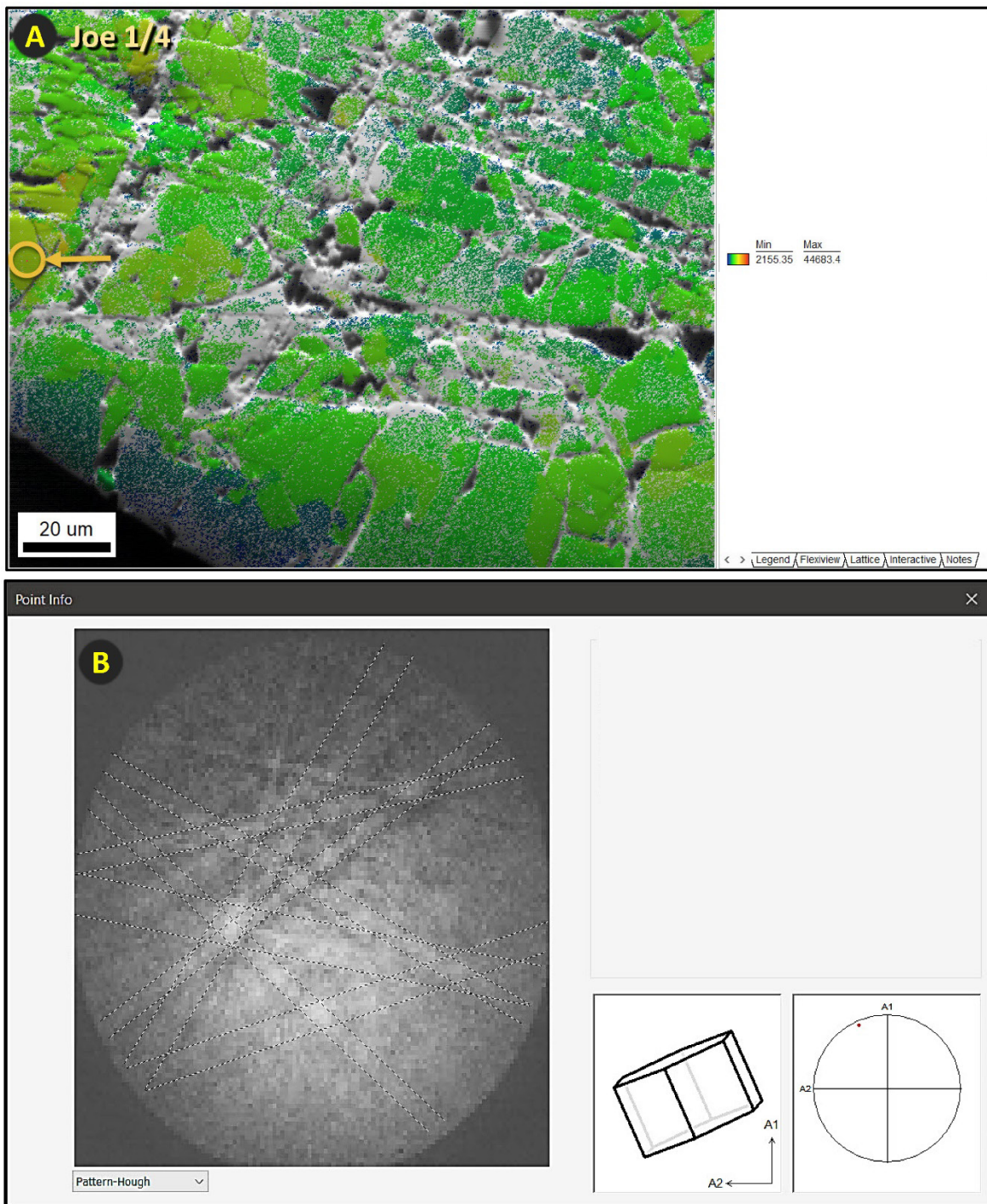
185
 186



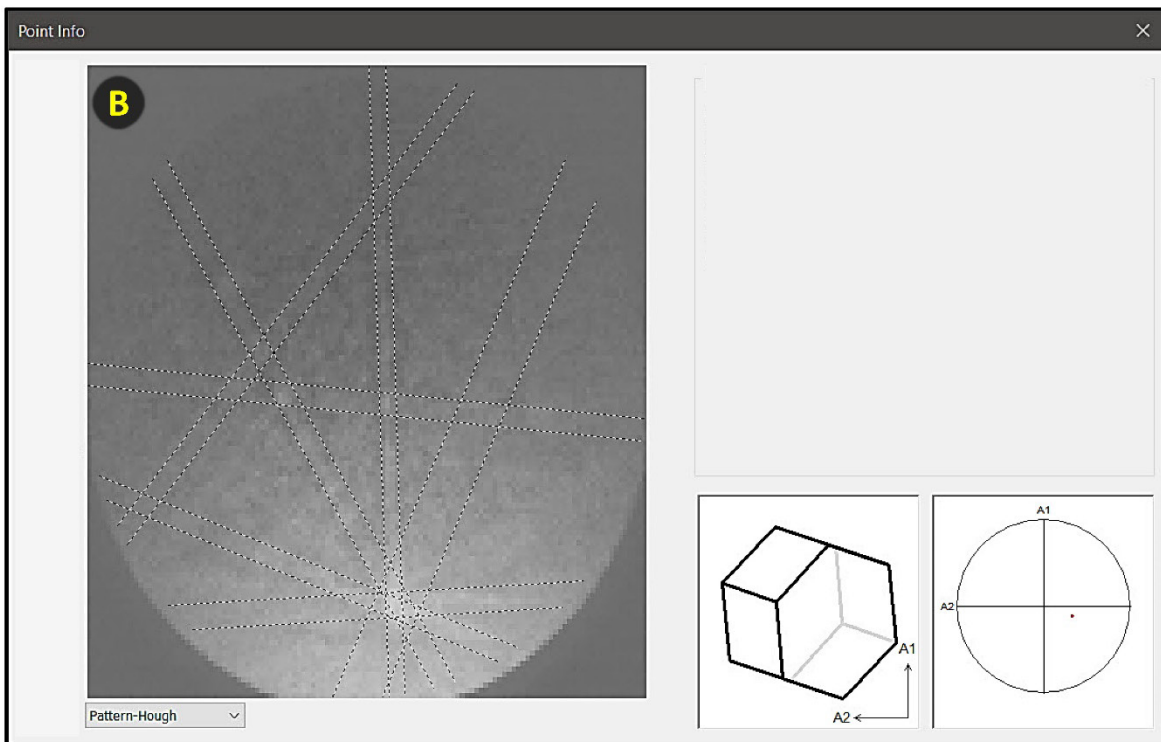
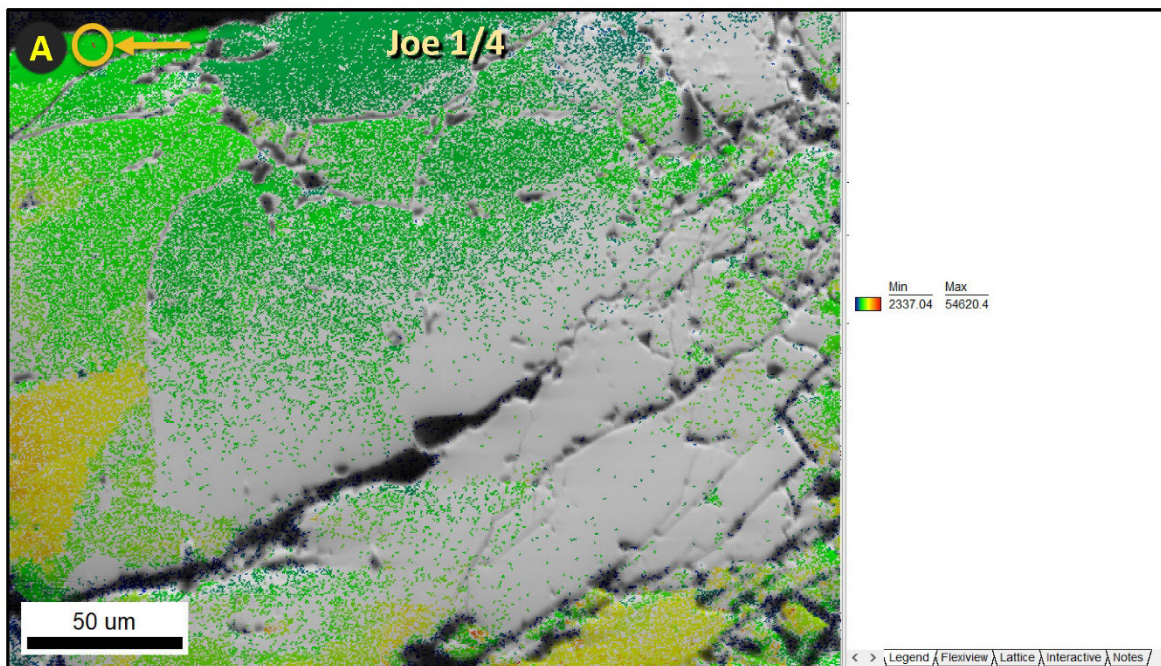
187
 188 **Figure S12. SEM-based EDS spectrum for Trinity meltglass grain 32x08.** For descriptions of
 189 panels (A)-(D), see the caption for Fig. S10.



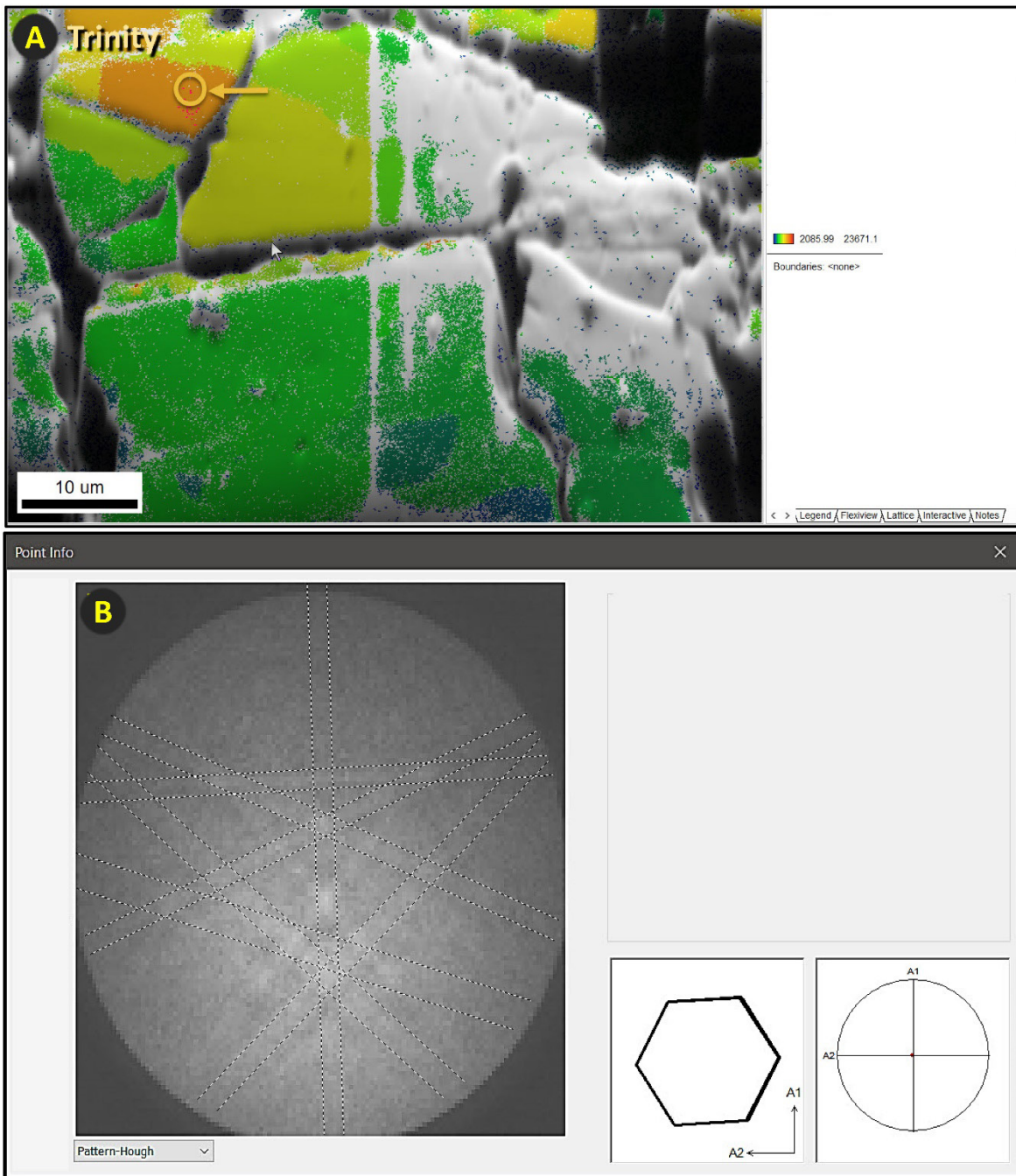
190
 191 **Figure S13. EBSD Kikuchi patterns of shock-fractured quartz.** (A) Meteor Crater grain 10x-
 192 12. EBSD image of virtual backscatter results (similar to SEM-BSE image) overlain by the grain
 193 average image quality. Blue/green/yellow/red colors denote decreasing image quality. Gray color
 194 represents areas where no Kikuchi patterns were detected, suggesting the area is amorphous or has
 195 short-range ordering of crystals. The gray area along the dashed yellow line is interpreted as a
 196 region of amorphous silica that intruded into the grain or melted *in situ*. (B) For EBSD analyses,
 197 the diffracted electrons produce what are called Kikuchi patterns that reveal the microstructural
 198 properties of the sample. The panel shows an EBSD Kikuchi pattern from a spot in the yellow
 199 circle in panel A. The lattice diagram at the lower right represents the grain's crystalline structure
 200 in which the hexagonal surface is the basal plane (0001), with the c-axis perpendicular to it.



201
 202 **Figure S14. EBSD Kikuchi patterns of shock-fractured quartz. (A)** Joe-1/4 grain 14x-04B.
 203 EBSD image of virtual backscatter results (similar to SEM-BSE image) overlain by the grain
 204 average image quality. Blue/green/yellow/red colors denote decreasing image quality. Gray color
 205 represents areas where no Kikuchi patterns were detected, suggesting the area is amorphous or has
 206 short-range ordering of crystals. **(B)** EBSD Kikuchi pattern from a spot in the yellow circle in
 207 panel A. The lattice diagram at the lower right represents the grain's crystalline structure in which
 208 the hexagonal surface is the basal plane (0001), with the c-axis perpendicular to it.



209
 210 **Figure S15. EBSD Kikuchi patterns of shock-fractured quartz. (A)** Joe-1/4 grain 19x-12C.
 211 EBSD image of virtual backscatter results (similar to SEM-BSE image) overlain by the grain
 212 average image quality. Blue/green/yellow/red colors denote decreasing image quality. Gray color
 213 represents areas where no Kikuchi patterns were detected, suggesting the area is amorphous or has
 214 short-range ordering of crystals. **(B)** EBSD Kikuchi pattern from a spot in the yellow circle in
 215 panel A. The lattice diagram at the lower right represents the grain's crystalline structure in which
 216 the hexagonal surface is the basal plane (0001), with the c-axis perpendicular to it.
 217



218
 219 **Figure S16. EBSD Kikuchi patterns of shock-fractured quartz. (A)** Trinity meltglass grain
 220 32x08. EBSD image of virtual backscatter results (similar to SEM-BSE image) overlain by the
 221 grain average image quality. Blue/green/yellow/red colors denote decreasing image quality. Gray
 222 color represents areas where no Kikuchi patterns were detected, suggesting the area is amorphous
 223 or has short-range ordering of crystals. **(B)** EBSD Kikuchi pattern from a spot in the yellow circle
 224 in panel A. The lattice diagram at the lower right represents the grain's crystalline structure in
 225 which the hexagonal surface is the basal plane (0001), with the c-axis perpendicular to it.

226
 227

228 **REFERENCES**

229

- 230 1. Stöffler, D.; Langenhorst, F. Shock metamorphism of quartz in nature and experiment: I.
231 Basic observation and theory. *Meteoritics* **1994**, *29*, 155-181.
- 232 2. Bunch, T.E.; LeCompte, M.A.; Adedeji, A.V.; Wittke, J.H.; Burleigh, T.D.; Hermes,
233 R.E.; Mooney, C.; Batchelor, D.; Wolbach, W.S.; Kathan, J.; et al. A Tunguska sized
234 airburst destroyed Tall el-Hammam a Middle Bronze Age city in the Jordan Valley near
235 the Dead Sea. *Sci Rep* **2021**, *11*, 1-64.
- 236 3. Gratz, A. Deformation in laboratory-shocked quartz. *Journal of non-crystalline solids*
237 **1984**, *67*, 543-558.
- 238 4. Gratz, A.J.; Fislser, D.K.; Bohor, B.F. Distinguishing shocked from tectonically deformed
239 quartz by the use of the SEM and chemical etching. *Earth and Planetary Science Letters*
240 **1996**, *142*, 513-521.
- 241 5. Blenkinsop, T. Shock-induced microstructures and shock metamorphism. *Deformation*
242 *Microstructures and Mechanisms in Minerals and Rocks* **2000**, 80-89.
- 243 6. Bohor, B.; Betterton, W.; Krogh, T. Impact-shocked zircons: discovery of shock-induced
244 textures reflecting increasing degrees of shock metamorphism. *Earth and Planetary*
245 *Science Letters* **1993**, *119*, 419-424.
- 246 7. Bohor, B.; Fislser, D.; Gratz, A.J. Distinguishing between shock and tectonic lamellae
247 with the SEM. In Proceedings of the Lunar and Planetary Science Conference, 1995; p.
248 145.
- 249 8. Hamers, M.; Drury, M. Scanning electron microscope-cathodoluminescence (SEM-CL)
250 imaging of planar deformation features and tectonic deformation lamellae in quartz.
251 *Meteoritics & Planetary Science* **2011**, *46*, 1814-1831.
- 252